







# Integration of geoelectric and electromagnetic methods to delineate subsurface mineralization in bostonite rocks, South El-Atshan area, Central Eastern Desert, Egypt

Hussein F. ABDELSALAM , Mohamed H. M. YOUSEF ,  
Mohamed A. SHAHEEN , Hassan M. BADR ,  
Ali M. EL-HAWARY , Ibrahim M. AL-ALFY\* 

Nuclear Materials Authority, Cairo, Egypt

**Abstract:** Bostonite rocks are widely spread in the Central Eastern Desert (CED) of Egypt, they are found in the form of sills or dykes injected in the Precambrian rocks. Postgeosynclinal (Hammamat) sediments were intruded by Postorogenic bostonites. The study of this area, using ground geophysical methods, aimed at tracking the radioactive mineralization under the surface, based on the possible association of this radioactive mineralization with some other mineralizations such as sulphides. The application of the self-potential survey shows that the highest negative anomalies are associated with the South El-Atshan bostonite sill and its contact zones. The depths to the centres of some selected anomalies range from 5.7 m to 24 m, half-widths oscillate from 6 to 32 m, with shallow dips towards the west and east directions. The horizontal-loop electromagnetic (HLEM) survey, which was conducted using four frequencies, revealed the presence of two conductive bodies. These conductive bodies possess narrow widths and depths, ranging from 25 m to 27 m, dipping towards the west direction with shallow angles of 25° and 40°, respectively. In addition, the induced polarization (IP) profile shows high chargeability values reaching more than 7.9 mV/V at depths starting from about 10 m to about 35 m. This zone corresponds to a high-resistance zone that may reflect a subsurface disseminated mineralization. The integration of the results obtained using the three techniques makes it possible to determine the most appropriate zones for the development of exploration in the area of investigation.

**Key words:** self-potential, electromagnetic, induced polarization, South El-Atshan, CED, Egypt

## 1. Introduction

Bostonite rocks were recorded in the Central Eastern Desert (CED) of Egypt as dykes and sills injected in the host Precambrian Hammamat sed-

\*corresponding author, e-mail: ibelalfy@yahoo.com

iments. The age of the bostonites is  $273 \pm 20$  Ma, i.e., Late Carboniferous to Early Permian (*El-Manharawy, 1972*). These bostonites represent one of the important igneous rocks that host uranium and/or thorium minerals. They can be divided into Th-rich and U-rich bostonites (*Mahdy et al., 1994*). The anomalies in bostonite rocks are mostly discovered in the region of Wadi Kareim–Wadi El-Dabbah, including the occurrences of Kareim–Oweirsha area (*Ibrahim, 1968*) and Wadi El-Tarfawy–Wadi El-Dabbah area (*El-Kassass, 1969*). The results of the detailed radiometric investigations (*El-Kassass, 1969*) discovered 83 radioactive anomalies, 80 of which are related to the bostonite rocks, and three anomalies are associated with slates and siltstones of the Hammamat sediments. Besides, this study revealed that the bostonite rocks cut the Hammamat sediments and most of the highly-radioactive bostonite bodies are striking in the N–S, NNE–SSW, and ENE–WSW directions.

El-Atshan area has been investigated geologically by *Obrenovic et al. (1966)*, *El-Kassass (1969)*, and *Dawood et al. (2004)* classified these rocks as trachytes on the basis of their geochemical characteristics. *Abd El-Naby (2009)* studied El-Atshan trachyte (bostonite) dyke and concluded that an unidentified secondary Zr-rich silicate mineral, betafite, and liandratite are identified for the first time in the trachyte (bostonite) dyke of El-Atshan area.

Airborne total-count (TC) radiometric prospection has been systematically applied in the region, since 1962, followed by several ground studies on this TC radiometric region (*Meshref et al., 1963; El-Meliegy, 1988; El-Qassas, 2014*). Some ground geophysical studies were conducted on some radioactive-bearing bostonite localities (*Assran et al., 2007, 2014; El-Qassas, 2014*).

The bostonite in the south El-Atshan area represents an extension of the first-discovered uraniferous bostonite of El-Atshan locality. This area contains two recorded anomalies ranging in values from 50 to 200  $\mu\text{R/h}$  (*El-Kassass, 1969*). The investigation of uranium minerals on the surface and exploratory mining works at El-Atshan uranium prospect area, revealed the presence of some primary uranium minerals and their secondary alteration minerals, associated with some sulphides of copper, iron, zinc, lead, molybdenum, etc. (*Hussein and El-Kassass, 1972*).

Radioactive exploration methods provide a map of the surface distribu-

tion of radioactive elements, which do not exceed 50 cm in depth (*IAEA, 2003*). Therefore, to locate the radioactive mineralization under the surface, various methods were used, depending on the association of the radioactive mineralization with other mineralization. This mineralization, such as sulfides, accompanies the penetration of hydrothermal solutions into the contact zones between the bostonites and their surroundings. For this reason, this area was selected for the ground geophysical studies in a trial to follow the exposed surface radioactive mineralization at deeper depths and obtain information about the probable lateral and vertical extensions through the application of the self-potential (SP), horizontal-loop electromagnetic (HLEM) and induced polarization (IP) Resistivity geophysical methods.

The present study area is situated in the Central Eastern Desert of Egypt, to the south of Qift - Qusseir asphaltic road, at approximately 40 km from Qusseir city, situated on the western shore of the Red Sea. It lies at the intersection of latitude  $25^{\circ} 49' 58''$  N and longitude  $34^{\circ} 06' 50''$  E (Fig. 1a).

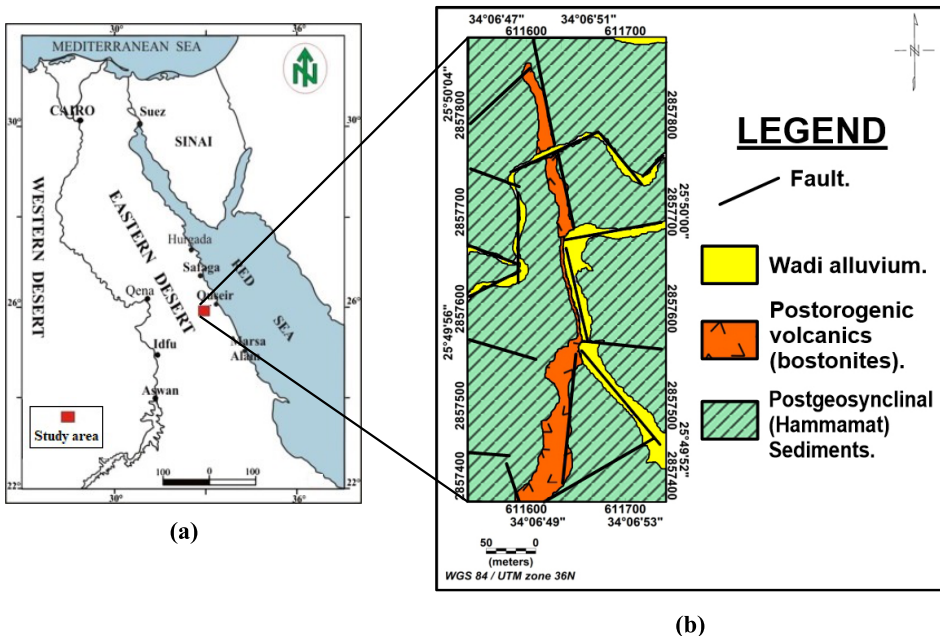


Fig. 1. Location map (a), geological map (b) of South El-Atshan area (modified after *El-Kassass, 1969*), Central Eastern Desert, Egypt.

## 2. Geologic setting

The rock units in the study area were classified according to *Hussein and El-Kassass (1972)*, depending on El-Shazly classification (*El-Shazly, 1964*), starting from oldest to newest into:

### 1. Postgeosynclinal (Hammamat) sediments:

They are represented by foliated siltstone (slate). They are fine-grained rocks, greyish green in colour, highly foliated and laminated, and their foliation planes are concordant with their bedding planes. Microscopically they are composed essentially of quartz, plagioclase feldspar, biotite and muscovite as thin small flakes, with subordinate chlorite and hornblende. These mineral grains are usually cemented by fine clayey minerals, dusty iron oxides and earthy carbonates, sometimes with microcrystalline silica.

### 2. Postorogenic volcanics:

They are represented by the bostonite rocks in the study area. They form a sill, emplaced along the bedding planes of the foliated siltstone, with a thin sheath of slaty rock at both upper and lower contacts (Fig. 1b). The sill has a variable thickness, ranging from 25 m to 35 m, with an average of 28 m (*Hussein and El-Kassass, 1972*), extending for about 1.5 km on the surface, with a general strike of N–S and moderate dip of  $40^\circ$  to the west and cut mainly by NE–SW faults.

Bostonite rocks are massive and consist of fine, buff-coloured grains, but the weathered parts are pale cream-yellow, with pitted surface, usually stained or filled with various alteration products, commonly including iron and manganese oxides, sometimes with carbonates and clayey materials, and so the rock became brown in colour. Microscopically, the bostonite is a holocrystalline rock. It is composed essentially of sodic feldspar laths, with some orthoclase crystals which form together about 80–90% of the whole rock, quartz does not exceed 5% and the ferromagnesian minerals are scarce, in the range of 5%. Zircon, apatite and violet fluorite are present as accessory minerals, together with the common deep red to black iron oxides.

Alteration features are well developed at the radioactive occurrences of El-Atshan, Um-Gir El-Atshan-II, and South El-Atshan bostonite (trachyte)

sills and/or dykes. Hydrothermal solutions altered both bostonite dykes as well as the surrounding rocks of Hammamat sediments. Hematitization and kaolinization are the most alteration features. They are described by *Hussein and El-Kassass (1980)*. The alterations are due to the action of hydrothermal activities, which took place later than the emplacement of the bostonite bodies and their deformation. These hydrothermal alterations are well noticed along the contact zones, where the bostonite rocks occurred and to a lesser extent in the enclosing foliated siltstone, which are highly altered. The thickness of this altered zone is not constant and reaches about 2.0 m or more through the bostonite rock, while in the foliated siltstone the zone of hydrothermal alteration does not apparently exceed 1.0 m.

### 3. Ground geophysical survey methods

#### 3.1. Self-Potential (SP) survey method

The method of measuring passive electrical potential distributed on the earth's surface with non-polarizable electrodes is called the self-potential (SP) method. Self-potential field surveys are conducted by measuring the electrical potential differences between pairs of electrodes that contact the surface of the Earth at a number of survey stations in the area of interest. These stations may be along profiles or spaced so as to obtain spatial coverage. With the self-potential method, the distribution of the electrical potential at the surface of the Earth (or in boreholes) is measured with respect to a reference electrode ideally placed at infinity (e.g. *Sato and Mooney, 1960*). One station is selected as a base station and all potentials are referenced to that point. Measurements are made by connecting a high-impedance voltmeter between at least two electrodes, usually the base station and a moving electrode. Data are plotted as profiles (observed potential versus distance along the profile) or, if the data provides sufficient coverage, as contour plots. As the method offers relatively rapid field data acquisition, it often is cost-effective for reconnaissance or initial investigation of an area prior to more intensive studies using other geophysical and geochemical techniques (*Telford et al., 1990; Parasnis, 1997*).

SP anomalies are associated with charge polarization mechanisms occurring at depth. The three main mechanisms are:

- (1) The streaming potential due to electrokinetic coupling (*Birch, 1998*),
- (2) the membrane or diffusion potentials due to chemical potential gradients of ionic species (*Maineult et al., 2004*), and
- (3) the “electro-redox” effect associated with redox potential gradients (*Naudet et al., 2004; Naudet and Revil, 2005*). Polarization results in the pores as a result of the gradient of chemicals carrying electrical charges.

The strong negative self-potential anomalies associated with the presence of ore deposits have been known since the nineteenth century (e.g. *Fox, 1830; Bølviken and Logn, 1975; Church, 1984; El-Kattan et al., 1996; Mousa et al., 2014; Assran et al., 2018; Grobbe and Barde-Cabusson, 2019; Horo et al., 2023*).

The SP survey was conducted along 13 profiles trending in the E–W direction mainly perpendicular to the strike of the bostonite sill with profile spacing of 40 m and 20 m station separation (Fig. 2). One station was selected as a base station and all potentials were referenced to that point. The reference point was chosen outside the study area to be away from the probable mineralization zone, as well as far from any surface structures such as faults and fractures that may contain some clay deposits, and away from areas that may contain subsurface moisture such as Wadi sediments.

### 3.2. Horizontal Loop Electromagnetic (HLEM) survey method

Subsurface conductive zones can be deduced using horizontal-loop electromagnetic (HLEM) methods by changing frequency values or changing the interspace distances between transmitter and receiver (*Keiswetter and Won, 1997*). The method requires that a sample of the transmitted signal is sent along a wire to the receiver, where it is used to synchronize the phase of the receiver with the transmitter. This permits the receiver to remove the effect of the transmitter signal (primary field) and to split the remaining secondary field into two components. One phase with the primary field (in-phase component) and the second component is the portion of the secondary field, which lags the primary field by one-quarter cycle (90°-quadrature component). The real (in-phase) and the quadrature (out-of-phase) components of the resultant secondary electromagnetic field are recorded at several frequencies by a receiver coil, and their values are recorded as a percentage of

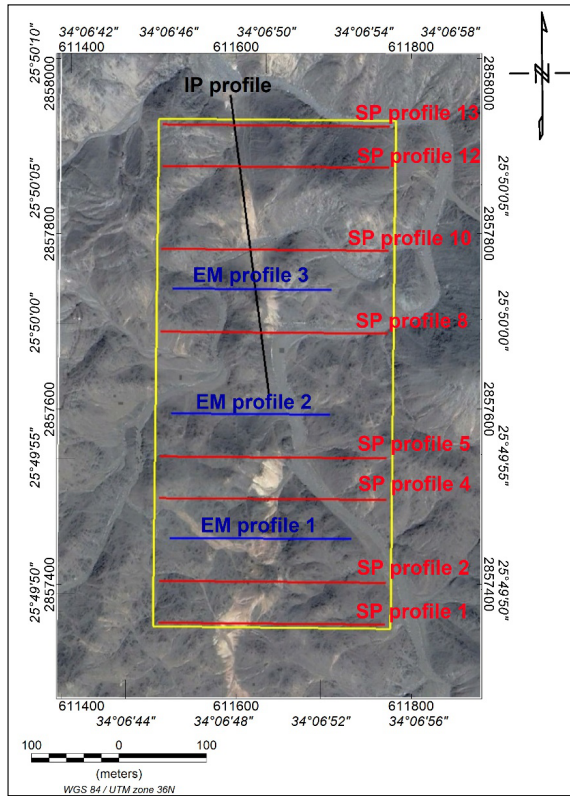


Fig. 2. Google Earth image showing self-potential (SP) survey area (yellow polygon), the selected SP profiles for quantitative interpretation (red lines), horizontal-loop electromagnetic (HLEM) profiles (blue lines), and induces polarization (IP) profile (black line), South El-Atshan area, Central Eastern Desert, Egypt.

the primary field. The midpoint joining the transmitter and receiver coils is considered as the point at which the conductivity is measured.

HLEM data were acquired using the APEX MAX-MIN I-8 instrument. To carry out the present HLEM survey, the two coils (transmitter and receiver) were separated by a fixed distance, which is 100 m coil separation and 20 m station separation. Three profiles were carried out trending in the E–W direction perpendicular to the strike of the bostonite sill (Fig. 2). In all measurements, four frequencies were used; 110 Hz, 440 Hz, 1760 Hz and 7040 Hz.

### 3.3. Induced Polarization (IP) survey method

Induced polarization is a current-induced electrical phenomenon observed as a delayed voltage in the earth materials (*Sharma, 1997*). Induced polarization is extensively applied due to its sensitivity to electronic and ionic conductors. It was developed to detect small concentrations of mineralization in the exploration of base metal, groundwater and geotechnical exploration (*Sumner, 1976; Parasnis, 1986; Anderson et al., 1990; and El-Sadek et al., 2021*). Application of the 2-D resistivity/IP method can give an image of both horizontal and vertical changes in the earth's properties and can be used in the identification of the structure and depth of buried features. *Yang et al. (2023)* stated that, low resistivity and high polarization can reflect the spatial occurrence of deep mineral structures and is used as an indirect clue for prospecting.

The basic equipment for the induced polarization (IP) survey consists essentially of a transmitter, a receiver, wires and electrodes. The data were collected using IRIS instrumentation. The transmitter used was a VIP 5000. It was powered by a Honda 5 kW motor generator. The receiver used was a six-channel model ELREC-6.

Time-domain induced polarization measurements (IP/resistivity) were conducted along one profile, using the dipole-dipole array, with dipole lengths of 20 m. This profile has a NNW–SSE direction, with a total length of 300 m (Fig. 2). It was performed from the north to the south, passing along the outcrop of the bostonite sill to follow the SP and HLEM anomalies and to ensure the detection of any subsurface mineralization.

Figure 2 illustrates a Google Earth image showing the location of the Self-potential (SP) survey area, the locations of the horizontal-loop electromagnetic (HLEM) lines, as well as the site of the induced-polarization (IP) profile.

## 4. Discussions and interpretations

### 4.1. Self-Potential (SP) survey

The results of self-potential survey (SP) are presented as a set of profiles (Fig. 3), plotting self-potential values are plotted against the distances of the measuring electrode from the base electrode. These profiles are usually



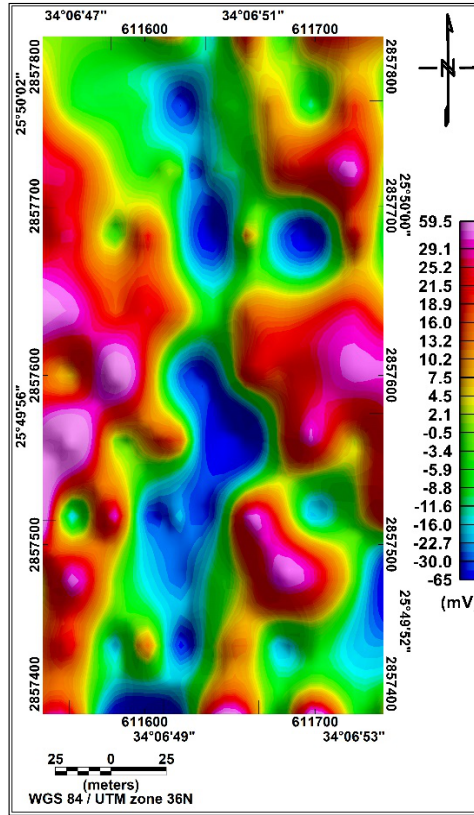


Fig. 3. Self-potential (SP) filled-colour map, South El-Atshan area, Central Eastern Desert, Egypt.

used to construct a contour map showing equipotential contour lines.

The SP contour map of the study area (Fig. 3) shows SP anomalous zones. Generally, the increase of SP negative values indicates the increase of the probable mineralization. The negative well-defined SP response associated with the bostonite sill, may be related to the content of possible mineralization. There is a good agreement between the SP contour map and the geological map (Fig. 1b). So, the SP map can assist in surface geological mapping.

The linearity of the individual SP anomalies reveals that the interpreted sheet-like bodies are controlled by the bostonite sill. High positive SP

anomalies reaching 61 mV are associated mainly with Hammamat sediments (slate) (Fig. 3). The relatively low positive SP values (0–16 mV) are associated with some parts of the slate. Relatively low to moderate negative SP values (–1 to –22 mV) are associated with the contact of bostonite sill with slate. The highest SP negative anomalies (–22 to –65 mV) occupy the central parts of the study area. These anomalies are associated with the bostonite sill and the lower and upper contact zones. The zones of the well SP anomaly (deep blue colour) are observed at the central part of the study area. There are some relatively high negative SP amplitudes, observed to the east of bostonite sill, which may be due to clay or poor conductive materials within the surface features as faults, or due to moisture on the narrow Wadi.

To obtain the causative body location, depth and dip, Babu and Rao method (Ram Babu and Atchuta Rao, 1988) was used to determine these parameters. It is a rapid graphical method for interpreting two-dimensional inclined sheets of finite depth extent. In the present study, nine anomalies, representing eight SP profiles (Nos. 1, 2, 4, 5, 7, 10, 12 and 13) were selected for the quantitative interpretations (Fig. 4). The obtained results from the nine selected SP anomalies are illustrated on Table 1.

Table 1. Results of the quantitative interpretation analysis for the nine SP anomalies, South El-Atshan area, Central Eastern Desert, Egypt.

Profile No. (Fig. 4)	Anomaly No. (Fig. 4)	Calculated parameters			
		$\theta$ (°)	Dipping direction	$h$ (m)	$a$ (m)
1	1	15	East	7.5	25
2	2	20	West	6	6
4	3	3	East	15	30
5	4	16	East	6.7	20
8	5	16	West	8	24
	6	20	East	8	13
10	7	25	East	24	32
12	8	10	West	5.7	19
13	9	5	East	5.8	20

$\theta$  = dipping angle in degrees,  $h$  &  $a$  = depth to the centre & half-width of the anomalous body in metres.

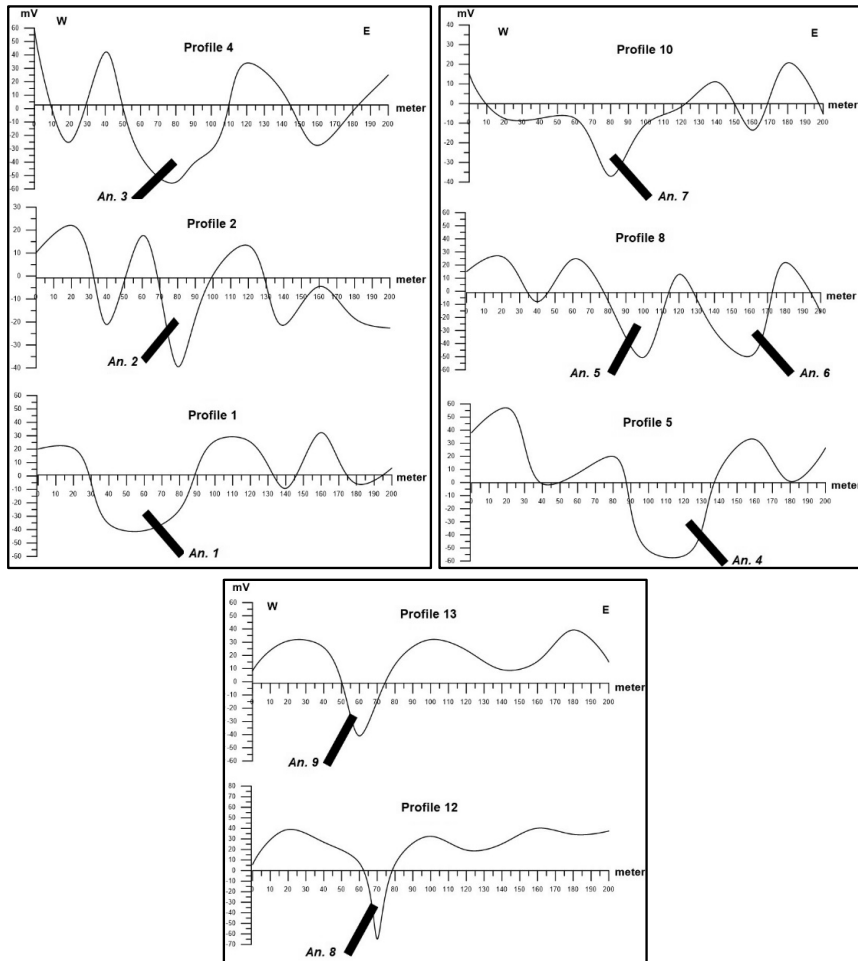


Fig. 4. Characteristic curves, with the calculated parameters of the SP profiles along E–W direction for nine SP anomalies, South El-Atshan area, Central Eastern Desert, Egypt.

#### 4.2. Horizontal Loop Electromagnetic (HLEM) survey

In field surveys, the in-phase response is particularly responsive to separated highly conductive bodies, while the out-of-phase component is normally used to infer the ground conductivities not to find conductive bodies. An efficient conductor will respond at progressively lower frequencies and a conductor will show negative in-phase values, whereas a poor conductor

will respond at only higher frequencies (*Keiswetter and Won, 1997*).

For the calculation of the ore bodies parameters for the horizontal-loop data, a half-plane is the most useful model for the very reason that it is the most common two-dimensional feature like a mineralized fissure, fault, vein, or conductive geological contact that is easily located in horizontal loop profiling (*Nair et al., 1974*). If the geometry of the body is simple, for example conductive zone around the fault plane, the depth to its upper edge and the product of the conductivity can be deduced from the negative peak values of the in-phase and out-of-phase components by using the type curves for the interpretation of Horizontal-Loop (*Ketola and Puranen, 1967*) and Standard curves for the interpretation of Horizontal-Loop EM anomalies (*Nair et al., 1974*). Also, the thickness or width of the conductive body is calculated from the relation between the two zero points of the (in-phase & out-of-phase components) and the distance between the two coils. In addition, the dipping angle can be calculated from the shape and values of the two positive peaks of (in-phase & out-of-phase components) using the same standard curves. Since frequency and coil spacing are known, the conductivity–thickness product can be obtained. The product has proved to be a useful measure of the economic value of the ore body.

Figure 5 illustrates the standard curves used to calculate the different HLEM parameters as *Nair et al. (1974)* described. The four main calculated parameters for the buried conductive body are the depth ( $d$ ), the dipping angle ( $\theta$ ), the width, and the conductivity thickness ( $\delta t$ ). Figure 5a used to estimate the body width by subtracting the coil separation from the anomaly width, while Fig. 5b used to calculate dip angle of the body using the two positive peaks for both the in-phase and the out-of-phase values, and the last curve (Fig. 5c) is used to estimate the two parameters  $d/a$  and  $\lambda/a$  to obtain the depth of the buried body ( $d$ ) and the conductivity thickness ( $\delta t$ ) from the equation:

$$\delta t = 10^5/a \mu f(\lambda/a),$$

where  $a$  is the coil separation,  $\mu$  is the magnetic permeability taken as unity, and  $f$  is the frequency (Hz) of the source.

### **Profile No. 1**

This profile (No. 1) is located at the southern part of the study area, trend-

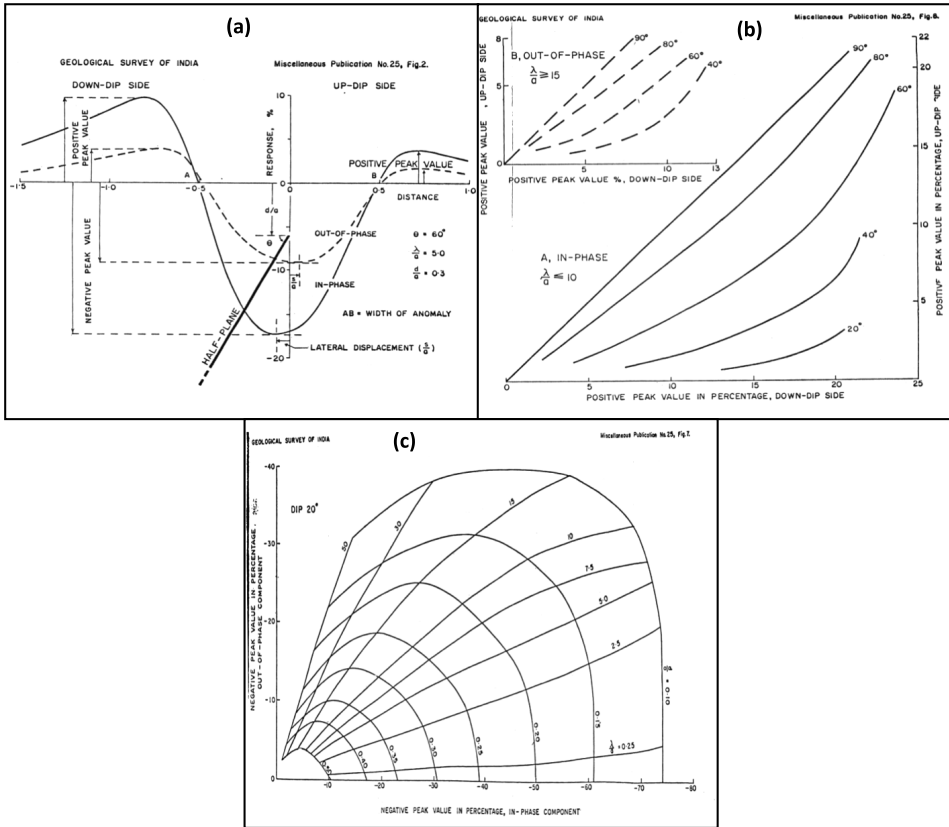


Fig. 5. Standard curves for the quantitative interpretation of HLEM data (Nair et al., 1974).

ing in a EW direction (Fig. 6a). This profile was carried out from west to east. The length of this profile is 160 m. The four frequencies used were 7040 Hz, 1760 Hz, 440 Hz, and 110 Hz.

Inspection of HLEM data acquired along this profile indicates the existence of negative in-phase component at the four frequencies in its eastern part (Fig. 6a). The in-phase component at the four frequencies reflects that the source of this anomaly is centred at station No. 150 and its opening towards east. This anomaly may be spatially related to the fault zone and is not due to a conducting body, which is confirmed by the positive to very weak negative out-of-phase component associated with this anomaly.

On the other hand, the negative response of the out-of-phase component spatially associated with the bostonite rock in the central part of the profile, which appears at the higher two frequencies may reflect ground conductivity with lithology change, without the presence of a conductive body, as evident from the relative stability of the in-phase component. This is consistent with the results of the self-potential (SP) survey, which show the presence of a weak negative anomaly in this location.

### **Profile No. 2**

This profile No. 2 was conducted with a length of 140 m and was conducted from west to east to detect and confirm the probable mineralization obtained from the Self-potential (SP) survey. Close examination of the two components of this profile (Fig. 6b) shows that the in-phase components indicate that there is a conductive zone with a maximum negative peak centred at station No. 60. The shape of the in-phase components with the used frequencies for the conductive zone reveals that the causative source has relatively good intensities. The defined EM anomaly data at the four frequencies coincide with the anomaly of SP beneath this profile, which may reflect that the causative source is a good conductor, situated at a shallow depth. The shape of the in-phase component reveals that the conductive body has a thin width, a low dip ( $25^\circ$ ) to the west direction, as obtained from the master curves for the rapid evaluation of the dip of the half-plane conductor, the depth to its surface is 27 m., and the conductivity thickness is 0.23 Siemens/m.

### **Profile No. 3**

This profile No. 3 was carried out from west to east, with a length of 160 m, using the four frequencies. The investigation of the HLEM data of this profile (Fig. 6c) indicates two well-defined EM anomalies at the four frequencies, centred at stations Nos. 60 and 120.

The first anomaly has a negative peak centred at station No. 60 on the four frequencies. The amplitude of the in-phase component is negative and weak (about 20%). Meanwhile, the out-of-phase component shows a weak negative amplitude at low-frequency, and the negativity increases by increasing frequency. This may reveal that a good conductor is buried at a shallow depth. The 1760 Hz curve was selected in the calculations. A thin conductive body with a moderate dip ( $40^\circ$ ) to the west direction, the

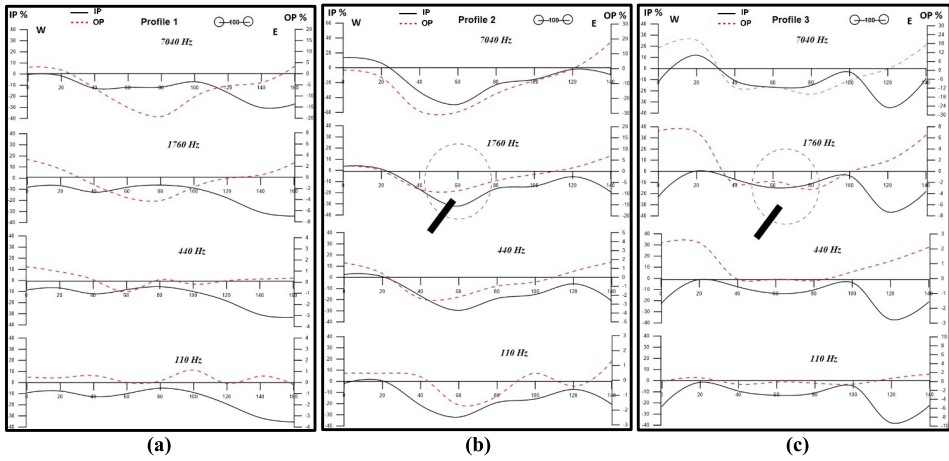


Fig. 6. Horizontal-loop electromagnetic (HLEM) profiles (a) profile No. 1, (b) profile No. 2, (c) profile No. 3, South El-Atshan area, Central Eastern Desert, Egypt.

depth to the surface of the conductor is 22 m, as revealed from the in-phase component. The conductivity thickness is 2.8 Siemens/m. Regarding the second anomaly, which is centred at station No. 120, a moderate negative is shown on the in-phase response of about 35 % and has no relationship in location to the bostonite sill. On the other hand, the out-of-phase component showed positive values. Therefore, this anomaly may be related to a conductive body located within a solid rock or due to a structural fault or fracture.

### 4.3. Induced Polarization (IP)

The IP/resistivity measurements are first viewed in a traditional 2-D measured apparent resistivity and chargeability pseudo-sections. They provide only a rather qualitative insight into the region of interest and can only cope with the traditional (surface linear – arrays, a set range of spacing) measuring schemes. Besides, pseudo-sections do not create particularly good images of the subsurface (Barker, 1981; Ulrich and Slater, 2004). So, calculation of resistivity and chargeability models helped constrain the interpretation of the field data to identify locations and orientations of anomalies.

The apparent electric resistivity and chargeability measurements were inverted into models using RES2DINV program (Loke, 2004). This pro-

gram automatically determines two dimensional (2-D) models for both resistivity and chargeability data that are obtained from IP/resistivity survey (Griffiths and Barker, 1993). This computer program uses the smoothness-constrained least-square inversion technique (Sasaki, 1992) to convert measured apparent IP/resistivity values to true resistivity and chargeability values and plot them on a cross-section (2D-model). On the  $x$ -axis is the distance along the surveying line and on the  $y$ -axis is the true depth (Fig. 7).

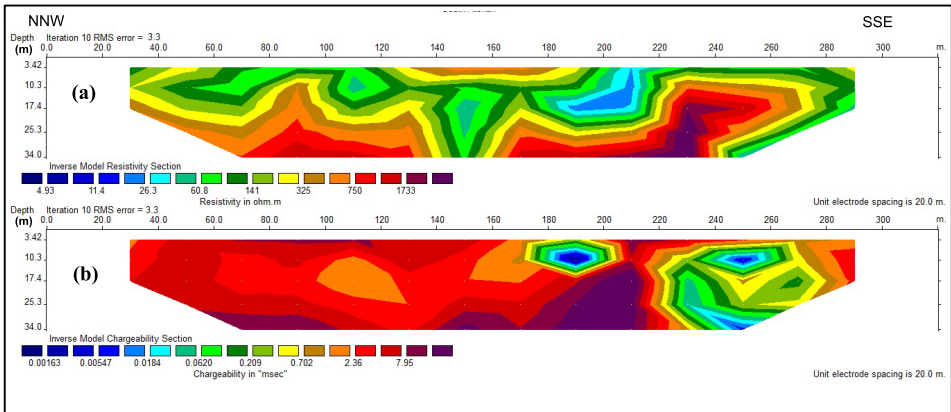


Fig. 7. Dipole-dipole sections of resistivity (a) and chargeability (b), with dipole spacing of 20 m, South El-Atshan area, Central Eastern Desert, Egypt.

The examination of the image resistivity model section of this profile (Fig. 7a) displays highly lateral and vertical changes all over the section from the surface down to a depth of about 35 m. The very high resistivity values (750 to >1733  $\Omega$ .m) are centred under stations Nos. 100 and 240. Four conductive zones are recorded on the resistivity model section (blue colour) of true resistivity values less than 140  $\Omega$ .m. The first zone is centred at station No. 80 and extends vertically from the near surface to a depth of about 17 m. The second zone is observed under station No. 110 and extends downwardly from the surface to a depth of about 15 m. The third zone is recorded at station No. 150 and extends vertically from a depth of 10 m to about 35 m. The fourth and last zone is centred at station No. 210, with a depth varying from near surface to about 20 m.

Figure 7b shows the chargeability model section of dipole length 20 m. The investigation of the chargeability model section displays two anomalous



zones of chargeability values, ranging between 2.3 mV/V and more than 7.9 mV/V. The first zone is centred under station No. 80, with a depth varying from 25 m to 35 m. The second zone is observed between stations Nos. 180 and 240, at depths starting from about 10 m to about 35 m, with very strong chargeability values of more than 7.9 mV/V. The second zone of high chargeability values corresponds to a high resistive zone, which may reflect possible and considerable subsurface disseminated mineralization beneath this part, which is still opening downwardly.

Therefore, a core drilling based on the geophysical results is recommended at station No. 200, with vertical drilling to a depth of 50 m to test depth, thickness and grade of mineralization.

Based on the present conducted studies in South El-Atshan area, CED, Egypt, an anomaly map was created showing the summary of the results of these three surveys (Fig. 8). This map shows the locations of the strongest anomalies according to the self-potential (SP) method, the locations of conductive bodies according to horizontal loop electromagnetic (HLEM) results, as well as the location of the highest chargeability zone according to the induced polarization (IP) method.

As illustrated on Figure 8, the black polygon surrounds the best location for work development in the study area through detailed trenching and exploratory drilling.

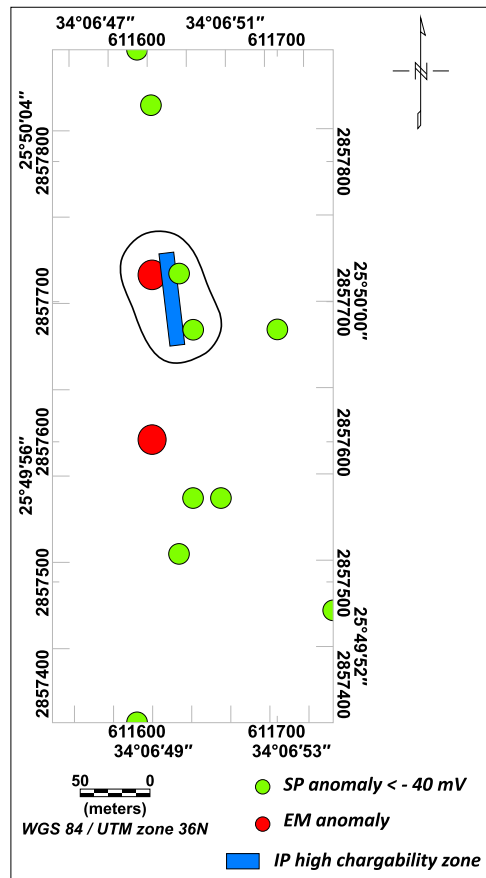


Fig. 8. SP, EM, and IP anomalies map, South El-Atshan area, Central Eastern Desert, Egypt.

## 5. Conclusions

The integration between the self-potential (SP), horizontal-loop electromagnetic (HLEM) and induced polarization (IP) methods in the study of South El-Atshan area helped much in obtaining important information about the lateral and vertical extensions of the previously-discovered surface radioactive mineralization. It is associated with bostonites and their contacts with the surrounding, depending on the association between this mineralization with some other mineralizations such as sulphides, as a result of post-magmatic hydrothermal processes. In general, the results of the study can be summarized in the following:

1. The SP measurements exhibit a wide range of amplitudes ( $-65$  mV to  $+60$  mV), with the highest negative values mainly along the bostonite sill and with the narrow Wadi. Quantitative interpretation of the SP data revealed shallow depths to the centres of nine selected anomalies, ranging from 5.7 m to 24.0 m and averaging 9.6 m. Meanwhile, the half-widths of the anomalous bodies range from 6 m to 32 m, with a mean value of about 21 m. All the anomalies have low dips; five anomalies dipping to the west and the other four to the east.
2. The application of the HLEM method revealed the presence of two conductive bodies, with different magnitudes. The two bodies are spatially associated with the bostonite sill and its contacts. The quantitative interpretation of the HLEM data revealed the existence of some conductive bodies possessing narrow widths, depths ranging from 25 m to 27 m, dipping towards the west direction, with shallow angles ranging between  $25^\circ$  and  $40^\circ$ , and conductivity thickness varying from 0.23 Siemens/m to 2.8 Siemens/m. All anomalies were recorded along the four frequencies, which may reflect shallow conductors that may represent deep mineralizations.
3. The results of using the induced polarization method showed the presence of a zone of high chargeability between the measuring stations Nos. 180 and 240, at a depth starting from about 10 m to about 35 m with strong chargeability values exceeding 7.9 mV/V. This zone corresponds to a high resistance zone, which may reflect disseminated mineralization distributed on the surface and subsurface below this part. This zone is

spatially related to high negative values of the self-potential, as well as to the presence of a good conductive body, as demonstrated by the results of using electromagnetic method. Accordingly, this area is considered a first priority in exploration development processes in the South El-Atshan area, CED, Egypt.

## References

- Abd El-Naby H. H., 2009: Role of geochemical alteration on the formation of secondary Zr- and U-bearing minerals in El-Atshan trachyte, Central Eastern Desert, Egypt. *J. Miner. Petrol. Sci.*, **104**, 1, 37–51, doi: 10.2465/jmps.080506.
- Anderson R., Bell B., Reynolds R., 1990: Induced polarization used for highway planning. In: Fink J. B., McAllister E. O. (Eds.): *Advances in applications and case histories of induced polarization*. SEG special publication.
- Assran S. M. A., Abuelnaga H. S. O., Khaleil A. F., 2007: Application of induced polarization, self-potential and magnetic techniques for the radioactive bostonite dykes of Wadi Rahia area, Central Eastern Desert, Egypt. Second International Conference on the Geology of the Tethys, Cairo University, Geizah, Egypt, **III**, 553–560.
- Assran A. S. M., Elsayed R. A. M., Ghazala H. H., Abdelsalam H. F., 2014: Gamma-ray spectrometry and induced polarization studies for El-Atshan-II uranium prospect area, Central Eastern Desert, Egypt. *Geomaterials*, **4**, 3, 92–104, doi: 10.4236/gm.2014.43010.
- Assran A. S. M., Yousef M. H. M., Hassan N. F., Abd El Salam H. F., 2018: Self-potential, electromagnetic and gamma-ray spectrometric studies for Abu-Shihat area, North Eastern Desert, Egypt. *Egypt. J. Appl. Geophys.*, **17**, 2, 1–12.
- Barker R. D., 1981: The offset system of electrical resistivity sounding and its use with a multicore cable. *Geophys. Prosp.*, **29**, 1, 128–143, doi: 10.1111/j.1365-2478.1981.tb01015.x.
- Birch F. S., 1998: Imaging the water table by filtering self-potential profiles, *Groundwater*, **36**, 5, 779–782, doi: 10.1111/j.1745-6584.1998.tb02195.x.
- Bølviken B., Logn Ø., 1975: An electrochemical model for element distribution around sulphide bodies. In: Elliot I. L., Flecher W. K. (Eds.): *Geochemical Exploration 1974*, pp. 631–648, Elsevier, Amsterdam.
- Church B. N., 1984: Geology and self-potential survey of the Sylvester K gold-sulphide prospect (82E/2E). In: *Geological fieldwork, 1983; A summary of field activities: British Columbia Ministry of Energy, Mines and resources paper 1984-1*, pp. 7–14.
- Dawood Y. H., Abd El-Naby H. H., Sharafeldin A. A., 2004: Influence of the alteration processes on the origin of uranium and europium anomalies in trachyte, Central Eastern Desert, Egypt. *J. Geochem. Explor.*, **88**, 1-3, 15–27, doi: 10.1016/S0375-6742(03)00210-3.
- El-Kassass I. A., 1969: Comparative geological investigation of the radioactive mineralization in the central Eastern Desert, Egypt. M.Sc. Thesis, Faculty of Science, Ain Shams University, Cairo, Egypt, 132 p.

- El-Kattan E. M., Adulhadi H. M., Rabie S. I., Hassanein H. I., 1996: Application of ground geophysical data to uranium mineralization in the El-Missikat area, central Eastern Desert, Egypt. *J. Afr. Earth Sci.*, **22**, 1, 81–91, doi : 10.1016/0899-5362(95)00120-4.
- El-Manharawy M. S., 1972: Isotopic ages and origin of some uranium bearing volcanic rocks in Egypt. M.Sc. Thesis, Faculty of Science, Cairo University, Cairo Egypt, 195 p.
- El-Meliegy M. A. M., 1988: Interpretation of aerial radiometric and magnetic survey data and their implications on the geology and structural pattern of the Central Eastern Desert of Egypt. Ph.D. Thesis, Faculty of Science, Ain Shams University, Cairo, Egypt. 237 p.
- El-Qassas R. A. Y., 2014: Airborne and ground geophysical studies for the mineralized bostonite rocks in Wadi El-Tarfawy – Wadi El-Dabbah area, Central Eastern Desert, Egypt. Ph.D. Thesis, Fac. Sci., Menoufiya University, Shibein El Koam, Egypt. 204 p.
- El-Sadek M. A., Al-Alfy I. M. M., El-Salam H. F. A., Zaeimah M. A. M., 2021: Ground electromagnetic and electric studies for Um-Salim gold mine, Central Eastern Desert, Egypt. *J. Geosci. Environ. Prot.*, **9**, 8, 129–139, doi : 10.4236/gep.2021.98008.
- El-Shazly E. M., 1964: On the classification of the Precambrian and other rocks of magmatic affiliation in Egypt. U. A. R. International Geological Congress, India, Part 10, pp. 88–101.
- Fox R. W., 1830: On the electromagnetic properties of metalliferous veins in the mines of Cornwall. *Philos. Trans. R. Soc. Lond.*, **120**, 1830, 399–414.
- Griffiths D. H., Barker R. D., 1993: Two-dimensional resistivity imaging and modeling in areas of complex geology. *J. Appl. Geophys.*, **29**, 3-4, 211–226, doi : 10.1016/0926-9851(93)90005-J.
- Grobbe N., Barde-Cabusson S., 2019: Self-potential studies in volcanic environments: A cheap and efficient method for multiscale fluid-flow investigations. *Int. J. Geophys.*, **2019**, 1, Article ID 2985824, doi : 10.1155/2019/2985824.
- Horo D., Pal S. K., Singh S., Srivastava S., Biswas A., 2023: New insights into the gold mineralization in the Babaikundi–Birgaon axis, North Singhbhum Mobile Belt, Eastern Indian Shield using magnetic, very low-frequency electromagnetic (VLF-EM), and self-potential data. *Minerals*, **13**, 10, 1289, doi : 10.3390/min13101289.
- Hussein H. A., El-Kassass I. A., 1972: Occurrence of some primary uranium mineralization at El-Atshan locality, Central Eastern Desert, Egypt. *J. Geol. U.A.R.*, **14**, 97–110.
- Hussein H. A., El-Kassass I. A., 1980: Some favourable host rocks for uranium and thorium mineralization in Central Eastern Desert, Egypt. *Ann. Geol. Surv. Egypt*, **10**, 897–908.
- Ibrahim A. B., 1968: Geology of radioactive occurrences in El-Kereim/El-Oweirsha area, Central Eastern Desert, U. A. R. M.Sc. Thesis, Faculty of Science, Ain Shams University, Cairo, Egypt 199 p.

- International Atomic Energy Agency (IAEA), 2003: Guidelines for radioelement mapping using gamma-ray spectrometry data. IAEA-TECDOC-1363, Vienna, Austria, 179 p.
- Keiswetter D., Won I. J., 1997: Multi-frequency electromagnetic signature of the cloud chamber, Nevada test site. *J. Environ. Eng. Geophys.*, **2**, 2, 99–103, doi: 10.4133/JEEG2.2.99.
- Ketola M., Puranen M., 1967: Type curves for the interpretation of Slingram (Horizontal Loop) anomalies over tabular bodies. Report of investigations No. 1, Geologinen Tutkimuslaitos, Geological Survey of Finland.
- Loke M. H., 2004: Tutorial: 2-D and 3-D electrical imaging surveys. Geotomo Software, Res2dinv 3.5 Software, 128 p.
- Mahdy M. A., Salman A. B., Assaaf H. S., 1994: Bostonite rocks as additional uranium resources in Egypt. In: Proc. 2nd Int. Conf. Geology of the Arab World, Cairo Univ., Geizah, Egypt, pp. 77–96.
- Maineult A., Bernabé Y., Ackerer P., 2004: Electrical response of flow, diffusion and advection in a laboratory sand box. *Vadose Zone J.*, **3**, 4, 1180–1192, doi: 10.2136/vzj2004.1180.
- Meshref W. M., Fouad K. M., Ammar A. A., Meleik M. L., 1963: Airborne radiometric prospection in the Eastern Desert, Egypt, Field Season 1962–1963, Internal Report (Unpublished), Geol. and Nuclear Raw Materials Dept., U.A.R. Atomic Energy Establishment, Cairo, Egypt.
- Mousa S. E. A., Elsayed R. A. M., Khalil A. F., Abd El-Nabi S. H., Yousef M. H. M., 2014: Delineating Cu-U mineralized zone in Wadi El-Regeita area, Southern Sinai-Egypt, using gamma-ray spectrometry and self-potential methods. *EGS J.*, **13**, 1, 115–125.
- Nair M. R., Biswas S. K., Mazumdar K., 1974: Standard curves for the interpretation of Horizontal Loop EM anomalies. *Geol. Surv. India, Miscellaneous Publication No. 25*.
- Naudet V., Revil A., Rizzo E., Bottero J.-Y., Bégassat P., 2004: Groundwater redox conditions and conductivity in a contaminant plume from geoelectrical investigations. *Hydrol. Earth Syst. Sci.*, **8**, 1, 8–22, doi: 10.5194/hess-8-8-2004.
- Naudet V., Revil A., 2005: A sandbox experiment to investigate bacteria-mediated redox processes on self-potential signals. *Geophys. Res. Lett.*, **32**, 11, L11405, doi: 10.1029/2005GL022735.
- Obrenovic M., El-Kassass I. A. E., El-Amein H. E., 1966: Report on the results of detailed exploratory mining works at the uranium deposit of Wadi El-Atshan locality, Central Eastern Desert, Egypt. Internal report, Atomic Energy Establishment, Cairo, Egypt.
- Parasnis D. S., 1986: Principles of applied geophysics, 4th Ed. Chapman and Hall, London, UK, 416 p.
- Parasnis D. S., 1997: Principles of applied geophysics, 5th Ed. Chapman and Hall, London, UK, 429 p.

- Ram Babu H. V., Atchuta Rao D., 1988: A rapid graphical method for the interpretation of the self-potential anomaly over a two-dimensional inclined sheet of finite depth extent. *Geophysics*, **53**, 8, 1126–1128, doi: 10.1190/1.1442551.
- Sasaki Y., 1992: Resolution of resistivity tomography inferred from numerical simulation. *Geophys. Prospect.*, **40**, 4, 453–463, doi: 10.1111/j.1365-2478.1992.tb00536.x.
- Sato M., Mooney H. M., 1960: The electrochemical mechanism of sulphide self-potentials. *Geophysics*, **25**, 1, 226–249, doi: 10.1190/1.1438689.
- Sharma P. V., 1997: Environmental and engineering geophysics. Cambridge University Press, 475 p.
- Sumner J. S., 1976: Principles of induced polarization for geophysical exploration, Volume 5. Elsevier, Amsterdam, Holland, 277 p.
- Telford W. M., Geldart L. P., Sheriff R. E., 1990: Applied geophysics, 2nd Ed. Cambridge University Press, 770 p.
- Ulrich C., Slater L., 2004: Induced-polarization measurements on unsaturated, unconsolidated sands. *Geophysics*, **69**, 3, 762–771, doi: 10.1190/1.1759462.
- Yang Y., Zhang G., Yao C., Deng Z., Ren Z., Li C., 2023: Application of induced polarization method in mineral resource exploration. *Sustainability*, **15**, 4, 3840, doi: 10.3390/su15043840.